Relaxation in a Natural Soil: Comparison of Relaxometric Imaging, $T_1 - T_2$ Correlation and Fast-Field Cycling NMR

S. Haber-Pohlmeier*[,1], S. Stapf[2], D. van Dusschoten[3] and A. Pohlmeier[4]

[1]*ITMC, RWTH Aachen University, Worringer Weg 1, Aachen, Germany;* [2]*Institute of Physics, Technical University Ilmenau, Germany;* [3]*ICG3, Research Centre Jülich, German;* [4]*ICG4, Research Centre Jülich, Germany*

Abstract: Longitudinal and transverse relaxation times are used to characterise the pore system of a natural Kaldenkirchen sandy loam. Here we present new results obtained by relaxometric imaging (MEMS) and two-dimensional T_1-T_2 correlation relaxometry, and compare these with available T_1- relaxation time distributions of water obtained by the analysis of fast field cycling relaxometry (FFC) data. The soil shows relatively broad bimodal distribution functions P(T_1) and P(T_2) with a T_1/T_2 ratio of about 2:1. The average T_1 as well as the spatial distribution, which are obtained from the relaxometric imaging corresponds well to the relaxometric results. From the analysis of the field dependent FFC data at low field including T_1 data obtained at high field the basic locally averaged relaxation mechanism is derived from the dispersion curve, i.e. the dependence of the relaxation rate from the magnetic field strength over five orders of magnitudes. From this we conclude that two-dimensional diffusion at locally flat surfaces controls the relaxation, i.e. the shapes of the distribution functions are controlled by surface relaxation.

Keywords: NMR, relaxometry, imaging, pore size distribution, Brownstein Tarr, T_1-T_2 correlation.

INTRODUCTION

Soils are natural porous media of highest importance for food production and maintenance of water resources. For these functions a prominent property is their ability to retain and transport water which is mainly controlled by pore size distribution. The latter is related to NMR relaxation times of the water molecules filling the pores, for which different measurement methods can be used. Most widespread are Carr Purcell Meiboom Gill (CPMG) for transverse relaxation and inversion or saturation recovery (IR, SR) for longitudinal relaxation (T_1) [1]. Besides this, T_1 can also be determined by Fast Field Cycling (FFC) [2] which allows investigations at variable field strength. Relaxometric methods can also be combined among themselves yielding correlation maps [3] or with imaging (MRI) leading to spatially resolved T_1 and T_2 times, which can also be analyzed statistically [4-9]. Generally, imaging methods contain more information than relaxation methods, since imaging resolves the information in two or three dimensions which is especially important for heterogeneous samples such as natural soil. But this is often paid by increased noise and a much smaller number of data points.

The aim of this study is to investigate the multimodal nature of the relaxation distribution functions observed in relaxation experiments of macroscopic samples at low fields and to find an answer to the question whether or not they are caused by macroscopic structures like fractures or by the inherent microscopic heterogeneity. For this purpose we measure T_1 and T_2 maps by relaxometric imaging and two-dimensional T_1-T_2 correlation maps and compare them with available data from fast field cycling relaxometry (FFC) experiments of a saturated natural sandy loam from Kaldenkirchen [10]. This will help in the future to better assess the information obtainable from magnetic resonance imaging which aims for understanding flow processes in natural soils.

*Address correspondence to this author at the ITMC, RWTH Aachen University, Worringer Weg 1, Aachen, Germany; Tel: +49(241) 80-264247; Fax: +49(241) 80-22185; E-mail: s.haber-pohlmeier@fz-juelich.de

MATERIAL AND METHODS

Sample Preparation

The Kaldenkirchen soil sample (73% sand, 23% silt, 4% clay, 0.25% Fe, 0.02% Mn, , 1% TOC) was sieved (<2mm) and filled, air-dry, into 9x100mm^2 quartz glass cuvettes which are closed at the bottom by a porous glass filter plate. The cuvettes were then centrifuged for 30 min at 3000rpm and finally wetted from the bottom for 48 h. The maximum water content was $\theta = 0.45$. Then the sample was sealed and measured by fast field cycling NMR relaxometry (FFC)[10], IR-CPMG, and imaged by a multislice-multiecho method (IR-MEMS).

Fast Field Cycling Relaxometry (FFC)

This method investigates the relaxation of an excited spin ensemble along the direction of the main magnetic field after a field jump [2]. The timing diagram is shown in Fig. (**1**). At the beginning the system is in thermal equilibrium corresponding to $B=B_{pol}$ or $B=0$, respectively. Then the field strength is switched quickly to B_{rlx}, but the spin ensemble does not follow instantaneously, i.e. the restoration of the new thermal equilibrium obeys a first order kinetic law with a characteristic relaxation time T_1. The polarization state of the ensemble is probed after varying time intervals τ, during which the sample is left at the magnetic field strength B_{relax}. This probing is performed by switching the magnetic field strength to B_{acq} and subsequently applying a 90° radio-frequency pulse. The free induction decay (FID) following this pulse is recorded and analyzed off-line in order to obtain

1874-7698/10

its amplitude, which is proportional to the magnetisation $M_z(\tau)$. A complete relaxation curve is then obtained by repeating the measurement cycle for different values of τ. In ideally homogeneous systems $M_z(\tau)$ is a single exponential function with a unique relaxation time T_1, in heterogeneous porous media multiple exponential functions are expected. The whole procedure may be repeated for different values of B_{relax}. All FFC measurements were performed on a Stelar Spinmaster (Stelar, Mede, Italy). T_1 relaxation curves were monitored at relaxation fields corresponding to Larmor frequencies of $\nu = \gamma B_{rlx}/2\pi$ = 20, 10.6, 5.6, 3, 1.6, 0.823, 0.435, 0.23, 0.121, 0.064, 0.034, 0.018, 0.009, and 0.005 MHz (γ is the gyromagnetic ratio of ^{1}H). The data are analysed by 1D inverse Laplace transformation [3].

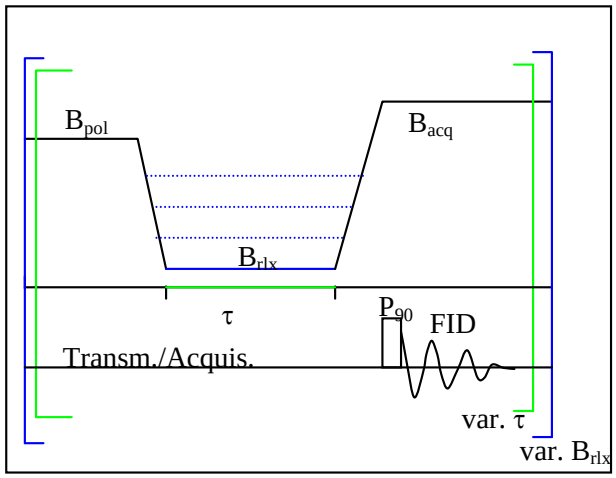

Fig. (1). Fast Field Cycling Method.

IR-MEMS NMR Imaging

The imaging experiments were performed on a 7T vertical bore magnet (Oxford Instruments, Oxford, UK), equipped with a Bruker (Karlsruhe, Germany) mini-imaging gradient set (G_{max} =300 mT/m), a 38mm rf birdcage coil, and a Maran DRX console. The used imaging sequence was a inversion recovery multiecho multislice sequence (IR-MEMS), which allows spatially resolved simultaneous determination of T_1 and T_2 relaxation times. A simplified timing diagram is displayed in Fig. (**2**).

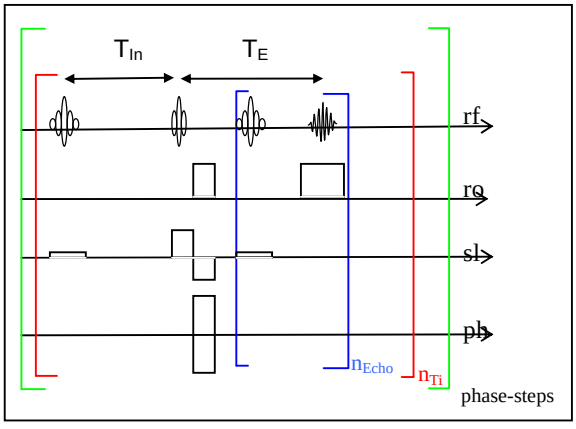

Fig. (2). Simplified IR-MEMS pulse sequence.

The basic idea of MEMS is a preparatory initial 180° pulse which inverts all magnetisation into –z direction. After a period t_{In} during which longitudinal relaxation evolves, a 90° slice selective soft pulse is applied which is followed by a CPMG echo train for the T_2 determination. This is repeated for several different inversion time periods. Due to the additional switching of phase "ph" and read-out "ro" encoding gradients the complete inversion-recovery CPMG pulse sequence becomes spatially resolved [3].

The signal intensity in each voxel obeys the following relation:

$$S(x,y,z,T_{In},T_E) = S_0(x,y,z)\left(1 - F\exp(-t_{In}/T_1)\right)\left(\exp(-nt_E/T_{2,app})\right) \quad (1)$$

with the inversion time t_{In}, the echo time t_E, the number of echoes n, and the longitudinal and apparent transverse relaxation times, T_1, and $T_{2,app}$. The transverse relaxation time T_2 is denoted as apparent since it comprises the true T_2 plus surface and diffusional effects. The prefactor F is theoretically 2, but in practice it should be fitted to the data in order to account for fast relaxation processes during the dead time of the receiver and effects of imperfect inversion pulses. Since soils possess quite fast apparent transverse relaxation times, $T_{2,app}$, we used the shortest adjustable value of t_E = 1.5 ms, which is paid by a relatively high slice thickness of 3mm. Further parameters were 0.009s < t_{In} < 1 s, t_R = 1.8s, FOV = 64x32 (32 x 16mm), and 14 axial slices scanned in interleaved mode. Original data $S(x,y,z,t_{In},nt_E)$ obtained for each voxel were fitted by Eq. 2, yielding maps (2D representations for chosen slices) of the physical quantities S_0, T_1, and $T_{2,app}$.

T_1-T_2 Correlation

The relation between longitudinal and transverse relaxation times can also be combined in a T_1-T_2 single NMR relaxation experiment. This is the non-spatially resolved version of IR-MEMS imaging and for the data analysis also Eq. 2 is valid. We have applied this method on the Kaldenkirchen soil sample described above in a 24 MHz Halbach low field scanner operated by a Stelar PC-NMR console (Stelar, Mede, Italy). t_E = 0.3ms, n = 512, 0.001s < t_{In} < 1s. The data are analyzed by 2D inverse Laplace transformation using Eq. (1) as kernel for Eq. (2):

$$M_z(\tau) = \iint P(T_1,T_2)\left(1 - 2\exp(-t_{In}/T_1)\right)\times \left(\exp(-nt_E/T_2)\right) dT_1 dT_2 + err \quad (2)$$

$P(T_1, T_2)$ is the unknown distribution function, the terms in brackets constitute the kernel, t_{In} is the inversion time, t_E is the echo time, n is the number of echoes, and err is an unknown error term [3, 11].

RESULTS

Fig. (**3**) shows T_1 and T_2 maps of four chosen axial slices of the saturated Kaldenkirchen soil sample. All regions from the soil give measurable and analyzable NMR signals. This means that this type of soil (sandy loam) is investigable by MRI which is not trivial since many soils show much shorter

transverse relaxation times due to small pore sizes and high content of paramagnetic ions [12]. The soil shows T_1 in the range of about 50 ms and T_2 of about 3 ms. Some spots with faster (green) and slower T_1 relaxation times (violet-white) are also present in the sample, especially near the top. T_2 appears more homogeneously. The long T_1 values in the top layer are caused by the somewhat smaller local packing density corresponding to larger pores.

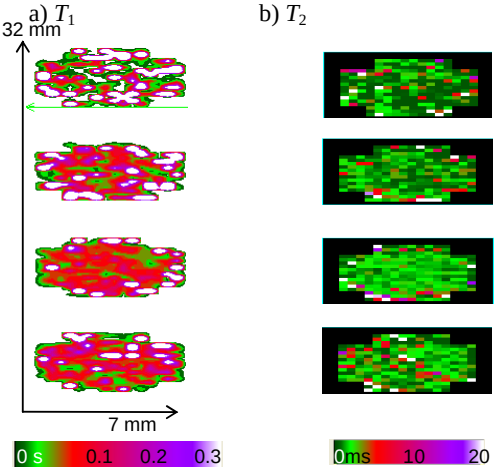

Fig. (3). T_1 and T_2 maps for the Kaldenkirchen soil sample at 7 T (ν_H= 300 MHz).

From the T_1 and T_2 maps relaxation time distributions are extracted by calculation of histograms of the populations of relaxation times in the soil, excluding the porous plate layer (Fig. **4**). T_2 shows a comparably narrow distribution in the range between 1 and 8 ms, with an average of 2 ms. But also voxels with higher T_2 (10 to 20 ms) exist, which are located near the edges. This is most probably due to packing faults at the soil-wall interface, where pores are larger. Also T_1 in these regions is longer. These effects may be interpreted by the Brownstein-Tarr model [13], which relates $1/T_{1,2}$ to the inverse pore size parameter Surface/Volume S/V, see Eq. 3 [10].

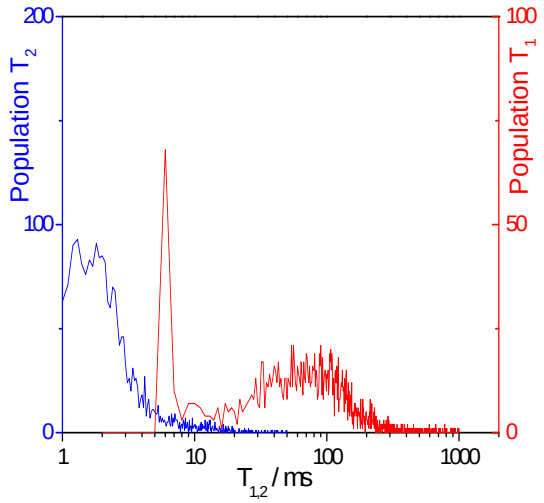

Fig. (4). T_1 (red) and T_2 (blue) histograms of the maps in Fig. (**3**).

T_1 shows a bimodal distribution, with a sharp peak at 7 ms and a broad mode between 10 and 300 ms. The sharp peak is near the shortest inversion time, and therefore must be interpreted with caution. It comprises all longitudinal relaxation processes faster than 10 ms, which are present, but not further resolved. The main mode is approximately log-normal distributed with $T_{1,mean}$ = 80 ms and a half width of log (T_1) = 0.3. T_2 depends strongly on t_E, so this is hard to compare. However, the reported relaxation times are in the range reported by Hall *et al.* [12] for several soils, e.g. Korkusova Hut sandy loam which has comparable texture with T_2 = 0.9 ms for t_E=1ms and t_1 = 90 ms at 40% saturation. It should be noted that Votrubova *et al.* [5] found for saturated soil also by statistical analysis of T_1 maps an average T_1 of 600 ms with a broad distribution over one order of magnitude. Issa *et al.* calculated T_1 relaxation time distributions for rocks in the same range [4]. Also a forest soil [14] with comparable texture shows similar relaxation times (5 and 45 ms at t_E = 0.3ms). The T_1 relaxation has been further investigated at lower Larmor frequencies between 5 kHz and 20 MHz by the FFC method.

Fig. (**5**) shows the measured relaxation curves, which are further analyzed by inverse Laplace transformation. The results are presented in Fig. (**6**). Clearly distinguishable are three processes: A broad main mode with average T_1 of 70 ms, which is accompanied by a faster relaxing component at about 10ms. Additionally, a small but very fast component at 2 ms is observed. Note that the limit of the shortest detectable T_1 component in the FFC experiments is about 1 ms. All modes shift simultaneously to faster times with decreasing Larmor frequency.

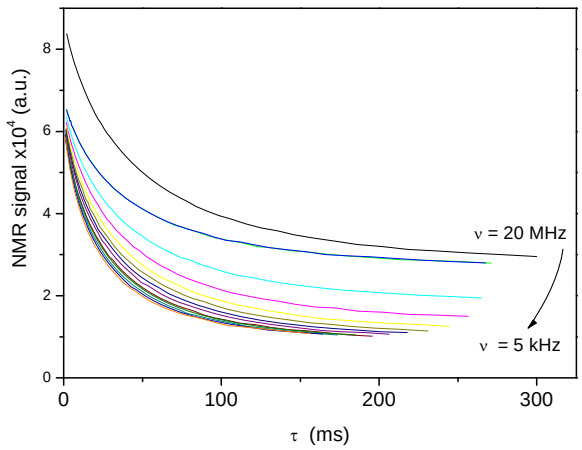

Fig. (5). T_1 relaxation curves at different Larmor frequencies for the saturated Kaldenkirchen soil sample, (modified, from [10]).

The data have already been analyzed further in terms of pore size distribution [10], where we found that the distribution of T_1 between 10 and 200 ms corresponds to pore sizes between one and some tens of microns using the Brownstein-Tarr model, see below. Here we include results from the high-field measurement into the analysis. The mean relaxation times for the main mode from FFC and MEMS measurements are plotted in Fig. (**7**). All data including the result at 300 MHz lie on one line. This indicates that the dis-

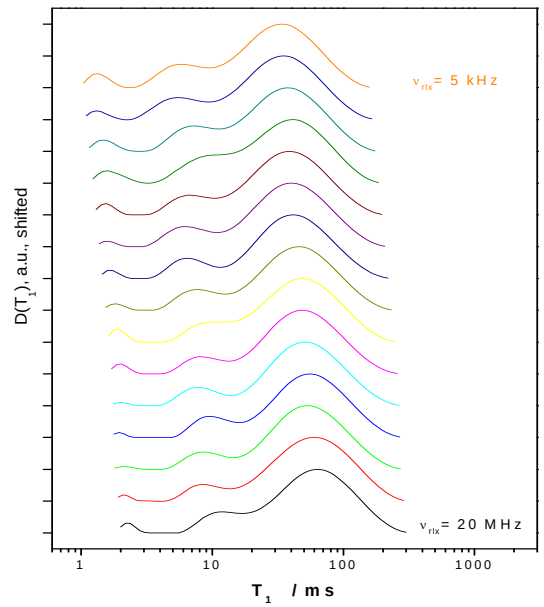

Fig. (**6**). T_1 relaxation spectra for Kaldenkirchen soil at different Larmor frequencies, normalized and offsetted (modified, from [10]).

persive behaviour follows the same frequency dependence in the whole observed range. The comparably weak dispersion and the linear relation between $1/T_1$ and the logarithm of the Larmor frequency ν_H indicates that the surface relaxation mechanism is controlled by local 2D diffusion processes at the pore walls [15].

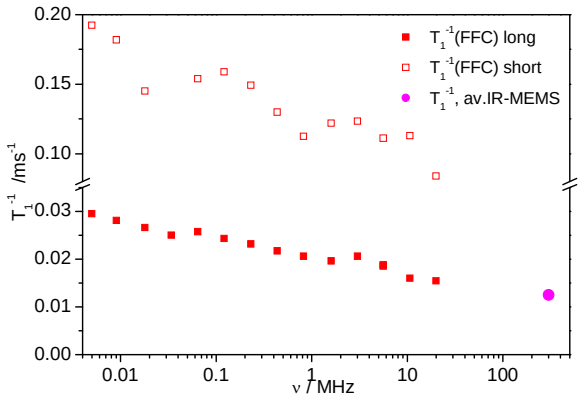

Fig. (**7**). T_1 relaxation at different Larmor frequencies from FFC (Fig. **6**) and MEMS T_1 map (Fig. (**4**)) (modified, from [10]).

Finally, the results are compared to a T_1-T_2 correlation experiment at ν_H = 24.3 MHz which is the non-spatially resolved version of the IR-MEMS experiment. The result is shown in Fig. (**8**). On the right facing axis labelled "nt_E" CPMG echoes are plotted, and the second, left facing axis, labelled "t_{In}", contains the different t_{In} values. The diagram should be read as an array of CPMG curves as a function of increasing inversion times t_{In}, during which T_1 relaxation evolves. The data are further analyzed by 2D inverse Laplace transformation using the program of Y.-Q. Song [3]. Fig. (**9**) shows bimodal distributions for both T_1 and T_2 which indicates two distinct pore size classes. The low amplitude spots at the limits of the inversion range are due to noise in the experimental data. The maxima for T_1 are at 20 and 90 ms and they correspond well to the FFC data for 20 MHz and the IR-MEMS data at 300 MHz (Fig. (**7**)). The main transverse relaxation modes at 9 and 50 ms are much slower than the T_2 modes identified at 300 MHz. As the echo time is much shorter at low field and the internal gradients are higher at high field this may be explained by the effect of molecular diffusion at high field.

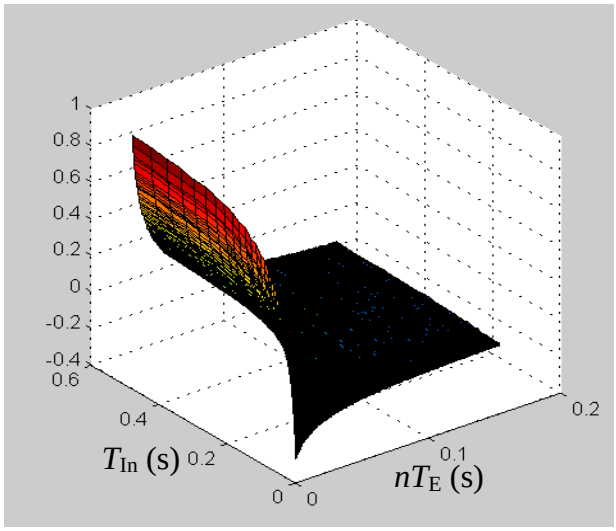

Fig. (8). T_1-T_2 correlation experiment on saturated Kaldenkirchen soil at ν_H = 24.3 MHz.

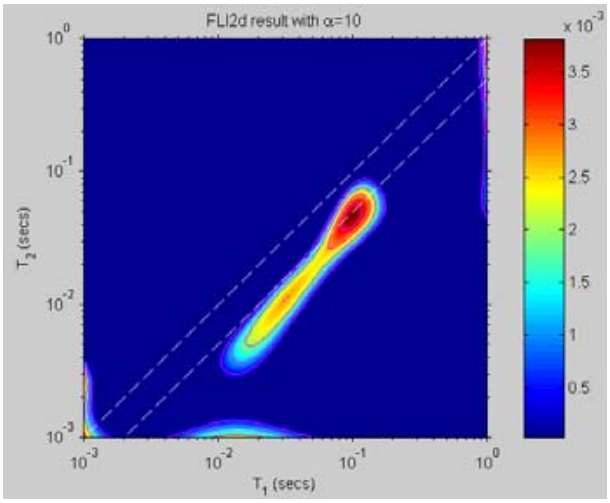

Fig. (9). T_1-T_2 correlation diagram of the data in Fig. (**8**) obtained by inverse 2D Laplace transformation, Eq. 2.

With decreasing T_1 (corresponding to decreasing pore sizes) the 2D distribution function shows an increasing ratio T_1/T_2 from two to three. These ratios agree well with several data obtained for porous media like rocks [16] and cements [17] and with theoretical considerations [17, 18]. An important observation is the lack of any detectable cross-peak contribution. A cross peak would indicate that for a give value

of T_1 two or more values of T_2 exist indicating multiple transverse relaxation mechanisms, so that T_2 is affected also by parameters other than pore size.

The general way to transform T_1 and T_2 distribution functions into pore sizes is the scaling by means of the Brownstein-Tarr equation:

$$\frac{1}{T_{1,2}} = \frac{1}{T_{1,2,bulk}} + \rho_{1,2}\frac{S}{V}, \quad (3)$$

incorporating an average surface relaxivity parameter $\rho_{1,2}$, which on its side is obtained from the average T_1, or T_2. This is obtained from the average surface/volume ratio S/V = 8300 cm^{-1} (from BET measurements, see [10]) as ρ_1 = 0.0023 cm s^{-1}. ρ_2 depends on t_E, we obtained ρ_2 = 0.0063 cm s^{-1} for the conditions of this investigation. Using these data the results from the 2D experiment in Fig. (**9**) can be recalculated into pore size distributions, shown in Fig. (**10**). The curves agree very well, although that obtained from T_2 is somehow broader.

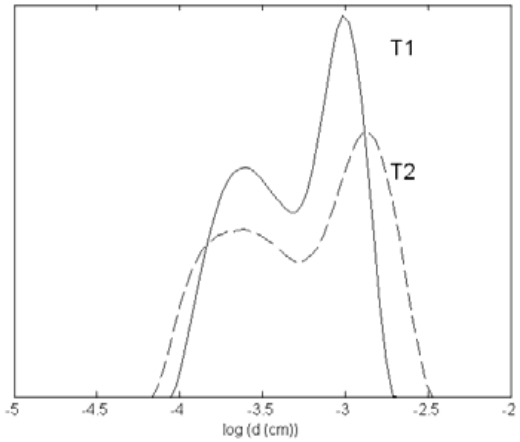

Fig. (**10**)**.** Pore diameter distributions obtained by projections on the T_1 and T_2 axis from the 2D experiment in Fig. (**9**). The relaxation times were rescaled to pore size distributions by means of the Brownstein-Tarr equation, the average S/V ratio from BET measurements [5], and assuming the capillary tube model.

The T_2 distribution obtained from imaging experiments is restricted due to t_E. A larger fraction of water in small pores relaxes during the first t_E period; a rescaling of T_2 distribution is meaningless, since it is strongly affected by internal gradients. One only can estimate the pore size limit, below which water is not detectable by MRI with these settings. With $T_{2,av}$ = 2 ms, one obtains $\rho_{2,300\ MHz}$ = 0.06 cm s^{-1}. Choosing $T_2 = t_E$ for the limiting value, one obtains $d_{limit} = 4V/S = 4\rho_2/(1/T_{2,limit}-1/T_{2,bulk}) \cong 4$ μm, assuming cylindrical pores. Please note also that this pore size limit corresponds to about the fast mode. A similar estimation for T_1 yields $\rho_{1,300\ MHz}$ = 0.0017 cm s^{-1} corresponding to a lower pore size limit of about 0.5 μm, if one uses a fastest detectable longitudinal relaxation time of 0.008s.

CONCLUSIONS

Kaldenkirchen sandy loam shows broad bimodal distribution functions of the longitudinal relaxation times T_1 over a large range of Larmor frequencies. A further very fast mode at around 2 ms is present but not well resolved. This short component probably corresponds to the clay components and represents strongly confined water in this phase. Similar short values have already been found in a different clayey soil [10]. The slow modes of T_1 at low magnetic fields correspond to the slow mode observed spatially resolved at high field (300 MHz). These modes are due to the relaxation in pores with a size in the range between 1 to some tens microns. The two slow modes (10 and 80 ms) are logarithmically dependent on the Larmor-frequency in the low field range and this continues for the slowest mode at high field of 300 MHz. According to Korb [15] this linear dependence on the logarithm of the Larmor frequency is interpreted as locally two-dimensional diffusion, where the basic relaxation mechanism is dipole-dipole interaction of water molecules with paramagnetic centres at the pore walls.

The spatially resolved relaxometric imaging method IR-MEMS generally yields additional information to the relaxometric measurements, although with inferior signal/noise ratio. This is mainly due to the smaller volumes over which the signal is integrated, i.e. a single voxel rather than the whole sample. The validity of the data is proven by the agreement between the average values from T_1 maps with T_1 determined relaxometrically. But T_1-mapping reveals structures which possess locally higher T_1 values in regions near the walls as well as near the top surface, i.e. the local pores are larger. This is due to packing faults near the walls and near the surface which are unavoidable for such natural samples.

The texture of the soil is finer than 2mm, no large grains are present, but aggregates of course. Water may penetrate into these aggregates, and contribute to the relaxation. The usage of 9 mm cuvettes and repacking the soil will definitely change the size of interaggregate pores. However, such pores are mainly macropores. So the macroporous structure of the soil will be changed due to the preparation and sample size. The meso- and microporous structures will be affected much less, so the relaxation time and pore size distributions reflect mainly this meso- and microporous structure, which are most responsible for the water storage of the soil, since the macropores are emptied firstly.

This study shows that T_1 mapping is a valuable tool for upcoming investigations of local pore size distributions in natural, i.e. undisturbed, soil cores for e.g. detection of preferential flow paths.

ACKNOWLEDGEMENTS

We thank N. Hermes, ICG-4, Research Centre Jülich for technical assistance and the DFG (SFB Transregional Collaborative Research Centre 32, PO-746-2/1 and Sta 511-4/1) for financial support.

REFERENCES

[1] Dunn KJ, Bergmann DJ, Latorraca GA. Nuclear magnetic resonance, petrophysical and logging applications. Pergamon: Amsterdam 2002.

[2] Kimmich R, Anoardo E. Field-cycling NMR relaxometry. Prog Nucl Magn Res Spectrosc 2004; 44: 257-320.

[3] Song Y-Q, Venkataramanan L, Hürlimann MD, Flaum M, Frulla P, Straley C. T1-T2 correlation spectra obtained using a fast two-dimensional laplace inversion. J Magn Reson 2002; 154: 261-8.

[4] Issa B, Mansfield P. Permeability estimation from T1 mapping. Magn Reson Imaging 1994; 12: 213-4.
[5] Votrubova J, Cislerova M, Amin MHG, Hall LD. Recurrent ponded infiltration into structured soil: a magnetic resonance imaging study. Water Resour Res 2003; 39: 1371.
[6] Edzes HT, van Dusschoten D, Van As H. Quantitative T-2 imaging of plant tissues by means of multi-echo MRI microscopy. Magn Reson Imaging 1998; 16: 185-96.
[7] Belliveau SM, Henselwood TL, Langford CH. Soil wetting processes studied by magnetic resonance imaging: correlated study of contaminant uptake. Environ Sci Technol 2000; 34: 2439-45.
[8] Cislerova M, Votrubova J, Vogel T, Amin MHG, Hall LD. Magnetic resonance imaging and preferential flow in soils. In: Van Genuchten MT, Leij FJ, Wu L, Eds. Characterization and measurement of the hydraulic properties of unsaturated porous media; U.S. Salinity Laboratory: Riverside CA 1997; pp. 397-411.
[9] Davies S, Hartwick H, Roberts D, Spowich K, Packer KJ. Quantification of oil and water in preserved rock by NMR spectroscopy and imaging. Magn Reson Imaging 1994; 12: 349-53.
[10] Pohlmeier A, Haber-Pohlmeier S, Stapf S. A fast field cycling NMR relaxometry study of natural soils. Vadose Zone J 2009; 8: 735-42.
[11] Provencher SW. A constrained regularization method for inverting data represented by linear algebraic or integral-equations. Comput Phys Commun 1982; 27: 213-27.
[12] Hall LD, Amin MHG, Dougherty E, *et al*. MR properties of water in saturated soils and resulting loss of MRI signal in water content detection at 2 tesla. Geoderma 1997; 80: 431-48.
[13] Barrie PJ. Characterization of porous media using NMR methods. Ann Rep NMR Spectrosc 2000; 41: 265-316.
[14] Schaumann GE, Hobley E, Hurrass J, Rotard W. H-NMR relaxometry to monitor wetting and swelling kinetics in high-organic matter soils. Plant Soil 2005; 275: 1-20.
[15] Korb JP, Bryant R. Magnetic relaxation dispersion in porous and dynamically heterogeneous materials. Adv Inorg Chem 2005; 57: 293-326.
[16] Schoenfelder W, Glaeser HR, Mitreiter I, Stallmach F. Two-dimensional NMR relaxometry study of pore space characteristics of carbonate rocks from a Permian aquifer. J Appl Geophys 2008; 65: 21-9.
[17] McDonald PJ, Korb JP, Mitchell J, Monteilhet L. Surface relaxation an chemical exchange in hydrating cement pastes: a two dimensional NMR relaxation study. Phys Rev E Stat Nonlin Soft Matter Phys 2005; 72: 011409.
[18] Kleinberg RL, Farooqui SA, Horsefield MA. T1/T2 ration and frequency dependence of NMR relaxation in porous sedimentary rocks. J Colloid Interface Sci 1994; 158: 195-8.

Received: August 17, 2009 Revised: December 11, 2009 Accepted: December 11, 2009